Journal of Energy Chemistry 71 (2022) 29–35

Contents lists available at ScienceDirect

Journal of Energy Chemistry

journal homepage: www.elsevier.com/locate/jechem

http://www.journals.elsevier.com/journal-of-energy-chemistry/

Dead lithium formation in lithium metal batteries: A phase field model

Rui Zhang [a,b], Xin Shen [c], Yu-Tong Zhang [a,b], Xia-Lin Zhong [c], Hao-Tian Ju [c], Tian-Xiao Huang [c], Xiang Chen [c], Jun-Dong Zhang [c], Jia-Qi Huang [a,b,*]

[a] Advanced Research Institute of Multidisciplinary Science, Beijing Institute of Technology, Beijing 100081, China
[b] School of Materials Science and Engineering, Beijing Institute of Technology, Beijing 100081, China
[c] Beijing Key Laboratory of Green Chemical Reaction Engineering and Technology, Department of Chemical Engineering, Tsinghua University, Beijing 100084, China

ARTICLE INFO

Article history:
Received 21 November 2021
Revised 9 December 2021
Accepted 10 December 2021
Available online 17 December 2021

Keywords:
Lithium metal batteries
Lithium metal anodes
Lithium dendrites
Dead lithium
Lithium stripping
Phase field methods
Finite element methods

ABSTRACT

Lithium metal batteries are the most promising choices for next-generation high-energy–density batteries. However, there is little mechanism understanding on lithium dendrite growth during lithium plating and the dead lithium (the main component of inactive lithium) formation during lithium stripping. This work proposed a phase field model to describe the lithium stripping process with dead lithium formation. The coupling of galvanostatic conditions enables the phase field method to accurately match experimental results. The factors influencing the dead lithium formation on the increasing discharge polarization are revealed. Besides, the simulation of the battery polarization curve, the capacity loss peak, and the Coulomb efficiency is realized. This contribution affords an insightful understanding on dead lithium formation with phase field methods, which can contribute general principles on rational design of lithium metal batteries.

1. Introduction

As the world pays ever-growing attention to green energy and carbon neutrality, the development of energy storage systems with high specific energy has become the key to the development of low-carbon energy. Among various types of secondary batteries, lithium metal batteries based on lithium metal anodes are one of the most promising batteries to achieve high specific energy. However, the instability of the lithium metal anode significantly hinders the practical application of lithium metal batteries. These issues are mainly attributed to the unstable lithium metal plating and stripping process with lithium dendrites and dead lithium, respectively, and commonly formed unstable SEI (solid electrolyte interphase), making lithium metal batteries meet challenges like poor cycle efficiency, short cycle life, and even security risks [1–3].

Realizing a controllable lithium metal plating and stripping process is the most critical step to improve the cycle efficiency and lifespan of lithium metal batteries [4–8]. The understanding on the mechanisms of the lithium metal plating and stripping process is still very scarce, especially the stripping process, which makes it difficult to achieve accurate construction of an effectively controlled lithium metal anode. The plating process of lithium metal is often accompanied by the growth of numerous lithium dendrites, which is mainly due to the extremely unstable interface of lithium metal and the retarded lithium-ion migration rate in electrolytes. During the stripping process, the lithium dendrites tend to dissolve unevenly, causing some metallic lithium to separate from the bulk lithium metal anode. The detached lithium metal, which is named dead lithium and also the main component of inactive lithium, cannot exchange electrons with the current collector, and is therefore unable to contribute its capacity in the subsequent cycles (Fig. 1). The formation of dead lithium will irreversibly lose the cycle capacity of the battery and reduce its Coulombic efficiency. Besides, the accumulated dead lithium in multiple cycles takes major responsibility for the pulverization of the lithium metal anode, which greatly shortens the cycle life of the lithium metal battery [9–16].

Compared with the massive research works on lithium dendrite growth during lithium plating, research on the dead lithium formation during the lithium stripping process is still scanty [17–33]. Various experimental technologies, such as *in-situ* optical microscopy [34], NMR (nuclear magnetic resonance) [35], *ex-situ* SEM (scanning electron microscope) [36], and TGC (titration gas chromatography) [37], have been proposed for qualitative or quantitative exploration of lithium stripping and dead lithium formation process [38–44]. However, it is extremely difficult to reveal the

* Corresponding author.
E-mail address: jqhuang@bit.edu.cn (J.-Q. Huang).

https://doi.org/10.1016/j.jechem.2021.12.020

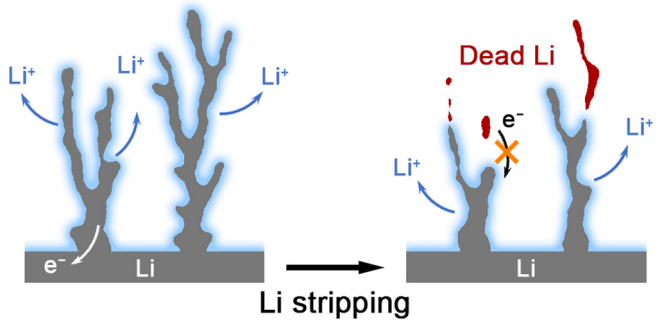

Fig. 1. The formation of dead lithium during the lithium stripping process.

structure–performance relationship between the dead lithium formation and the discharging electrochemical performance due to the limitation of the high instability of lithium metal and the high complexity and difficulty of *in-situ* accurate quantitative characterizations. While the experimental exploration is struggling, various theoretical models have been proposed to investigate the mechanism of the cycle process in lithium metal batteries, including density functional theory (DFT) [45], molecular dynamics (MD) simulation [46], Monte Carlo (MC) method [47], finite element method (FEM) [48], and phase field method (PFM) [49–53]. Among them, the phase field method has become the most accurate and effective theoretical model for quantitatively studying the mechanism of lithium metal anodes, due to its outstanding ability to accurately track the phase change interface evolution at the mesoscale. Based on the theoretical basis of the early established electrochemistry phase field theory [54,55,56], Chen *et al.* realized the Butler–Volmer equation coupled phase field model of the lithium dendrite growth [57,58]. After that, many phase field models emerged to investigate mechanisms of lithium metal anodes from the perspectives of structure design [59–62], mechano-electrochemical [63,64], thermal effect [65,66], *etc.* However, these theoretical calculations mainly explored the lithium plating process, and hardly involved the equally critical stripping process of lithium metal anodes, which is essential to construct lithium metal batteries with high cycle efficiency and long lifespan.

In this contribution, a phase field model on the lithium stripping process with dead lithium formation is constructed for the first time. The galvanostatic charge and discharge process of lithium metal anodes were also firstly simulated with phase field models. Such galvanostatic simulation conditions allow us to feel accurate morphology and electric potential evolution processes, which match the mainstream galvanostatic results in experiments, leading to mechanism conclusions with practical guiding significance.

2. Modeling method

The electrochemical reaction during the lithium plating and stripping process in lithium metal batteries can be illustrated as follows.

$$Li^+ + e^- \rightleftharpoons Li \tag{1}$$

In this two-phase system, there is both an electrolyte liquid phase containing lithium ions and a solid phase composed of lithium metal. Here, a phase field order parameter ξ is introduced to describe the phase change evolution of the two phases, where ξ = 0 denotes the electrolyte liquid phase, and ξ = 1 denotes the lithium metal solid phase. ξ varies from 0 to 1 in the interfacial region, representing a diffuse interface between lithium metal and electrolyte. It should be noticed that such diffuse interface is a numerical virtual interface, and does not refer to the actual SEI on lithium metal anodes.

Based on Chen's nonlinear phase field model and our previous works [49,57,59,63], the total free energy can be given by

$$F = \int_V \left[f_{ch}(c_i) + f_{grad}(\xi) + f_{elec}(c_i, \varphi) + f_{ns}(\xi)\right] dV \tag{2}$$

where $f_{ch}(c_i) = \sum c_i(RT \ln a_i + \mu_i^\theta)$ is the Helmholtz free energy density. c_i, a_i, and μ_i^θ are the concentrations, the activities, and the reference chemical potential of species i (for Li ions, anions, and Li atoms), respectively. R is the molar gas constant. T is the temperature. $f_{grad}(\xi) = \frac{1}{2}\nabla\xi \cdot \kappa\nabla\xi$ is the gradient energy density, and the gradient coefficient κ can be expanded as $\kappa(\theta) = \kappa_0[1 + \delta\cos(\omega\theta)]$, which is associated with the surface energy anisotropy. κ_0, δ, ω, and θ are the gradient energy coefficient, the anisotropy strength, the anisotropy mode, and the relative angle of the interface normal vector, respectively. $f_{elec}(c_i, \varphi) = F\varphi\sum z_i c_i$ is the electrostatic energy density, φ is the electrostatic potential, F is the Faraday's constant, and z_i is the valence of species i. $f_{ns}(\xi) = h'(\xi)\chi\psi$ is the noise term presenting the non-uniform interface. χ and ψ are the random number and the amplitude of fluctuation, respectively.

Coupled with Butler–Volmer kinetics, the partial differential equations that describe the temporal evolution of order parameter ξ can be deduced [57,59]. For lithium plating process

$$\frac{\partial\xi}{\partial t} = -L_\sigma\left(\frac{\partial f_0}{\partial\xi} - \kappa\nabla^2\xi + \frac{\partial f_{ns}}{\partial\xi}\right) - L_\eta h'(\xi)\left[\exp\frac{(1-\alpha)F\eta}{RT} - \frac{c_{Li^+}}{c_0}\exp\frac{-\alpha F\eta}{RT}\right] \tag{3}$$

where L_σ denotes the interfacial mobility, L_η denotes the reaction constant. $f_0(\xi) = W\xi^2(1-\xi)^2$ is an arbitrary double well function, where W/16 represents the barrier height between the two equilibrium states for electrode and electrolyte. $h(\xi) = \xi^3(6\xi^2 - 15\xi + 10)$ is an interpolating function. $1-\alpha$ and α are the anodic and cathodic charge transfer coefficients, respectively. $\eta = \varphi_s - \varphi_l - E_{eq}$ is the activation overpotential, φ_s, φ_l, and E_{eq} are the electrostatic potential in the lithium metal solid phase, the electrostatic potential in the electrolyte liquid phase, and the equilibrium potential (which equals to 0 in this model), respectively.

For lithium stripping process

$$\frac{\partial\xi}{\partial t} = -f_d L_\sigma\left(\frac{\partial f_0}{\partial\xi} - \kappa\nabla^2\xi + \frac{\partial f_{ns}}{\partial\xi}\right) - f_d L_\eta h'(\xi)\left[\exp\frac{(1-\alpha)F\eta}{RT} - a_{Li^+}\exp\frac{-\alpha F\eta}{RT}\right] \tag{4}$$

where $f_d = f_{step}(-\varphi_l/\varphi_d)$ is introduced as a variable to describe the active state of local lithium metal; $f_{step}(x)$ is a step function that steps from 1 to 0 when x is larger than 1; the reference potential φ_d is set as 1.0 mV, thus, $f_d = 1$ denotes active lithium, $f_d = 0$ denotes dead lithium. It is worth noting that the determination of the φ_d value here needs to be adjusted according to the specific model, which will significantly affect the accuracy of the description on the active state of lithium metal. $a_{Li^+} = h(c_{Li^+}/c_0)$ is introduced as the activity of Li ions, since the Li ion concentration is higher than 1.0 M during the lithium stripping process, suggesting that it is no longer suitable to approximate Li ion activity to Li ion concentration directly.

The partial differential equation that describe the temporal evolution of Li ion concentration is given as

$$\frac{\partial c_{Li^+}}{\partial t} = \nabla\cdot\left(D_{Li^+}\nabla c_{Li^+} + D_{Li^+}c_{Li^+}\frac{F}{RT}\nabla\varphi_l\right) - c_s\frac{\partial\xi}{\partial t} \tag{5}$$

where D_{Li^+} is the Li ion diffusion coefficient in electrolytes. c_s is the Li atom concentration in the lithium metal solid phase.The electro-

static potential in the lithium metal solid phase φ_s here is considered equal everywhere in the whole lithium metal solid phase, and only evolves over time, which is controlled by galvanostatic simulation conditions. The electric potential in the electrolyte liquid phase φ_l can be solved with Poisson's equation

$$\nabla^2\varphi_l = 0 \tag{6}$$

The galvanostatic simulation conditions are realized by introducing global equations, which solve two variables φ_s and $\varphi_{l,\mathrm{up}}$ by iterative method to keep the two equal signs in the following equation are always true during the whole lithium plating/stripping process

$$I_0 = I_\mathrm{r} = I_\mathrm{mt} \tag{7}$$

where $\varphi_{l,\mathrm{up}}$ is the maximum liquid phase potential difference of the model, that is, the electric potential boundary value at the upper boundary. I_0 is the constant areal current density as an input parameter of the model, taking positive and negative values during the charging and discharging process, respectively. I_r is the reaction areal current density. I_mt is the mass transfer areal current density.

$$I_\mathrm{r} = \frac{c_s F}{S}\int_V \frac{\partial\xi}{\partial t}\mathrm{d}V \tag{8}$$

$$I_\mathrm{mt} = \frac{F}{S}\int_S \vec{n}\cdot\left(D_{\mathrm{Li}^+}\nabla c_{\mathrm{Li}^+} + D_{\mathrm{Li}^+}c_{\mathrm{Li}^+}\frac{F}{RT}\nabla\varphi_l\right)\mathrm{d}S \tag{9}$$

where S is the projected area of the model in the vertical direction. $\vec{n}$ is the outward unit normal vector at the upper boundary.

This galvanostatic lithium plating and stripping phase field model was simulated by finite element method on COMSOL Multiphysics 5.5 platform. A two-dimensional model consisting of a 30.0 μm × 30.0 μm square domain is introduced. The maximum grid spacing is 0.5 μm. The upper boundary is considered as the bulk electrolyte with a constant Li ion concentration c_0 and a variable liquid phase electric potential $\varphi_{l,\mathrm{up}}$. The lower boundary acts as a current collector, where the liquid phase electric potential φ_l is set as 0. The parameters mentioned above are detailed in Table S1.

3. Results and discussion

The dendritic lithium plating morphology is the main prerequisite for the massive production of dead lithium in the lithium stripping process. In order to accurately quantitatively simulate the formation process of dead lithium, the lithium dendrite morphology was firstly generated with this galvanostatic lithium plating phase field model (Fig. 2a–c). By introducing the noise term $f_{\mathrm{ns}}(\xi)$ in consideration of the effect of the non-uniform surface energy, the tree-like lithium metal dendrites with inconsistent thickness, random bifurcation, and random kinks that are closer to the observed lithium dendrites by experiments can be simulated.

Taking the lithium dendrite morphology at 480.0 s of the lithium plating process as the initial morphology of the discharge lithium stripping process, the dead lithium formation during the galvanostatic lithium stripping process was simulated (Fig. 2d–f, Fig. S1). During the discharge process, a growing number of lithium metal pieces are separated from the bottom active lithium to form dead lithium. When the discharge time reaches 404.8 s, all active lithium is consumed, and the lithium stripping simulation ends automatically.

An in-depth analysis of the lithium stripping process at different discharge times is conducted (Fig. 3). In order to clearly distinguish between active lithium and dead lithium in phase field order parameter diagrams in Fig. 3(a–c), Fig. 3(d–f) exhibits a distribution map of active lithium and dead lithium, according to the introduced active state function f_d. The simulated dynamic process of dead lithium formation can be found in Movie S1. Obviously, the generation of dead lithium starts from the top first, since the lithium metal on dendrite tips is far away from the bottom current collector, and the uneven lithium dissolution process can easily render multiple dissolve sites on the dendrite waist. When the lithium metal detaches and becomes dead lithium, the internal

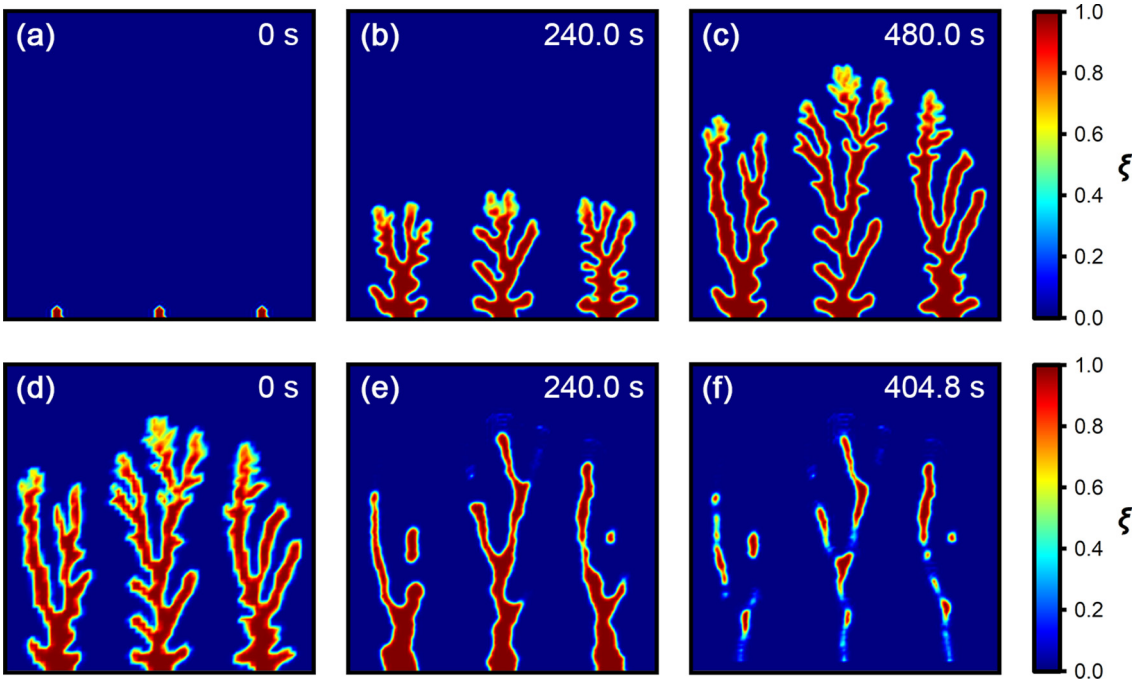

Fig. 2. Phase field simulations of the galvanostatic lithium plating and stripping processes. (a–c) Lithium dendrite growth at 0, 240.0, and 480.0 s, respectively, with a plating current density of 10 mA cm^{-2}; (d–f) Dead lithium formation process at 0, 240.0, and 404.8 s (cut-off time), with a stripping current density of 10 mA cm^{-2}.

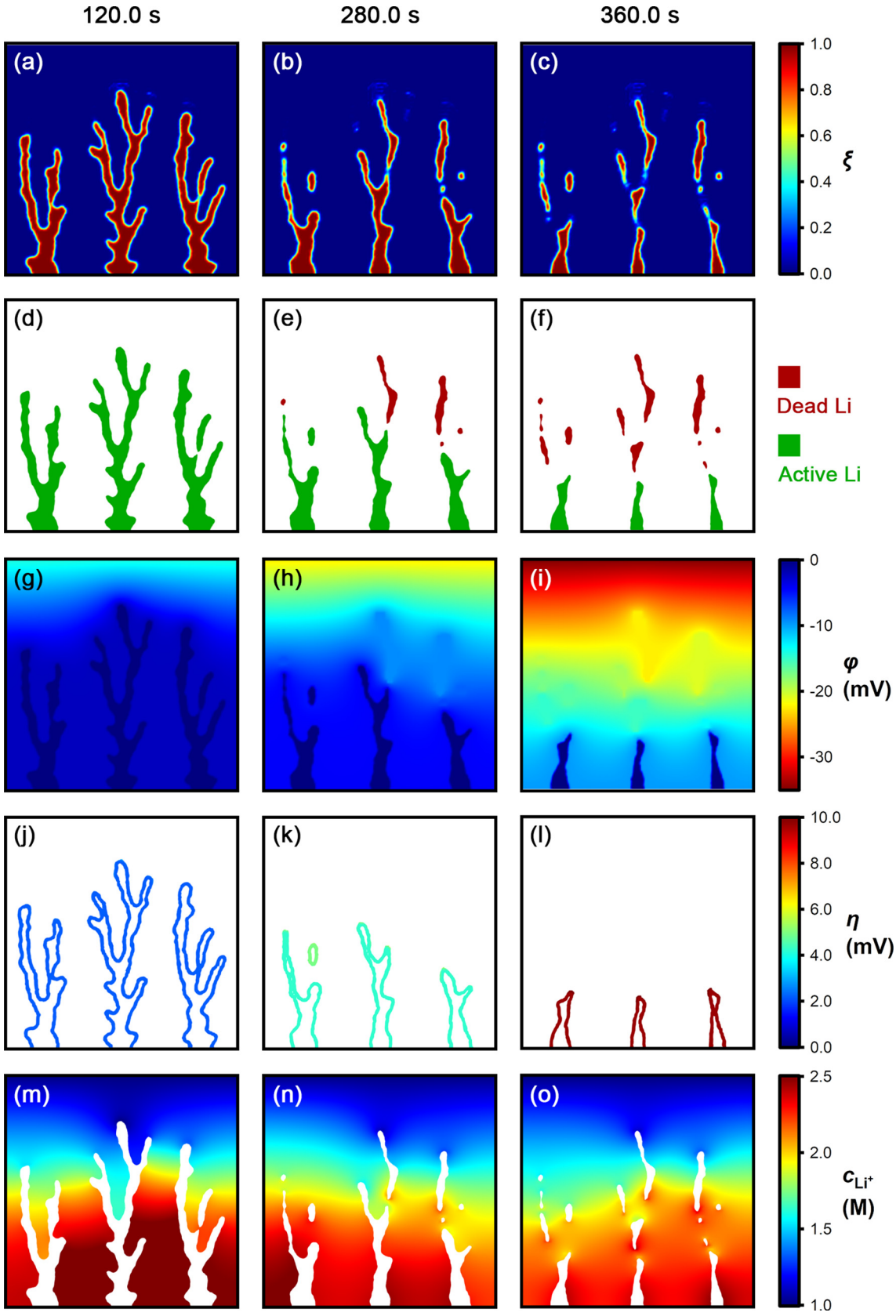

Fig. 3. The dead lithium formation processes. (a–c) Lithium stripping morphology evolution (phase field order parameter); (d–f) distribution of active lithium and dead lithium; (g–i) electrostatic potential evolution; (j–l) activation overpotential at the active lithium surface; (m–o) Li ion concentration in electrolytes at 120.0, 280.0, and 360.0 s, respectively.

electrostatic potential of the dead lithium will be consistent with the potential of the surrounding liquid electrolyte (Fig. 3g–i). Due to the high electrical conductivity of the lithium metal, the internal potential of each piece of dead lithium is consistent everywhere. Dead lithium has the same electrostatic potential as the surrounding electrolyte, and cannot transmit electrons to the current collector, so it is naturally unable to be oxidized and contribute its capacity. Besides, it is worth noting that under the condition of galvanostatic discharge condition, when dead lithium is formed, the surface area of active lithium will suddenly reduce, which makes the local areal reaction rate suddenly increase. Correspondingly, the activation overpotential that drives the electrochemical reaction will suddenly arise after the formation of dead lithium. As shown in Fig. 3(j–l), when no dead lithium is formed at 120.0 s, the average activation overpotential is only about 2 mV. When a small amount of dead lithium is formed at 280.0 s, the average activation overpotential increases to about 4 mV. When a large amount of dead lithium is formed at 360.0 s, the active surface area is greatly reduced, and the activation overpotential increases to over 10 mV. Furthermore, the Li ion concentration around the lithium dendrites will increase rapidly during the lithium stripping process (Fig. 3m–o, Fig. S2). According to the Nernst equation or Butler–Volmer kinetics, the increase of the Li ion concentration slows down the dissolution reaction rate of lithium metal under the same activation overpotential. Under the external galvanostatic condition, the rise of local Li ion concentration also aggravates the increase of activation overpotential. The significant reduction in the active surface area and the increase in the local Li ion concentration together significantly intensify the activation overpotential in the later stage of the dead lithium forming discharge process.

Both voltage and current curves of the full-cell or half-cell are always collected synchronously from a working battery during the cell discharge process. The capacity profile can be also obtained. It is difficult to analyze the specific lithium stripping process only with these curves. Based on phase field model results, the influence of the dead lithium formation on the electrochemical properties can be further revealed. The 8 largest dead lithium pieces are marked with serial numbers from (1) to (8) according to the formation sequence (Fig. 4a and b). Among them, the first piece of dead lithium is formed at 250.5 s. In the curves of total voltage and average activation overpotential, after the time the first piece of dead lithium formed, the activation overpotential begins to rise (Fig. 4c). Besides, the closer to the discharge cut-off time, the greater the influence of the dead lithium formation on the jump of activation overpotential. At the same time, the total voltage is also increased step by step in synchronization with the activation overpotential. The model employed herein is a half-cell with an equilibrium potential of 0 V, therefore the total voltage in the figure corresponds to the total polarization. When dead lithium is formed, it will significantly strengthen the battery polarization, especially at the end of the discharge process, where a tiny dead lithium formation will also greatly increase the polarization. In the capacity curves, the dead lithium capacity begins to appear after 250.5 s and gradually rises until 404.8 s when the active lithium capacity is reduced to zero with discharge cut-off (Fig. 4d). The Coulombic efficiency can be directly calculated as 83.1% (including the capacity of the existing lithium nucleation sites before the lithium dendrite growth in Fig. 2a). The capacity loss rate I_{loss} is defined as the first derivative of dead lithium capacity with respect to time (Fig. 4e). The loss peaks on the spectrum can clearly identify all dead lithium formation time points. Obviously, these peaks are in one-to-one correspondence with the potential step time points in Fig. 4c. Therefore, by analyzing the total voltage curve or polarization curve obtained in experiments, the rapid identification of the dead lithium formation can be realized. Experiments usually provide only the total polarization and the total capacity curves, the mechanisms behind the electrochemical properties can be revealed in detail through phase field theory simulations.

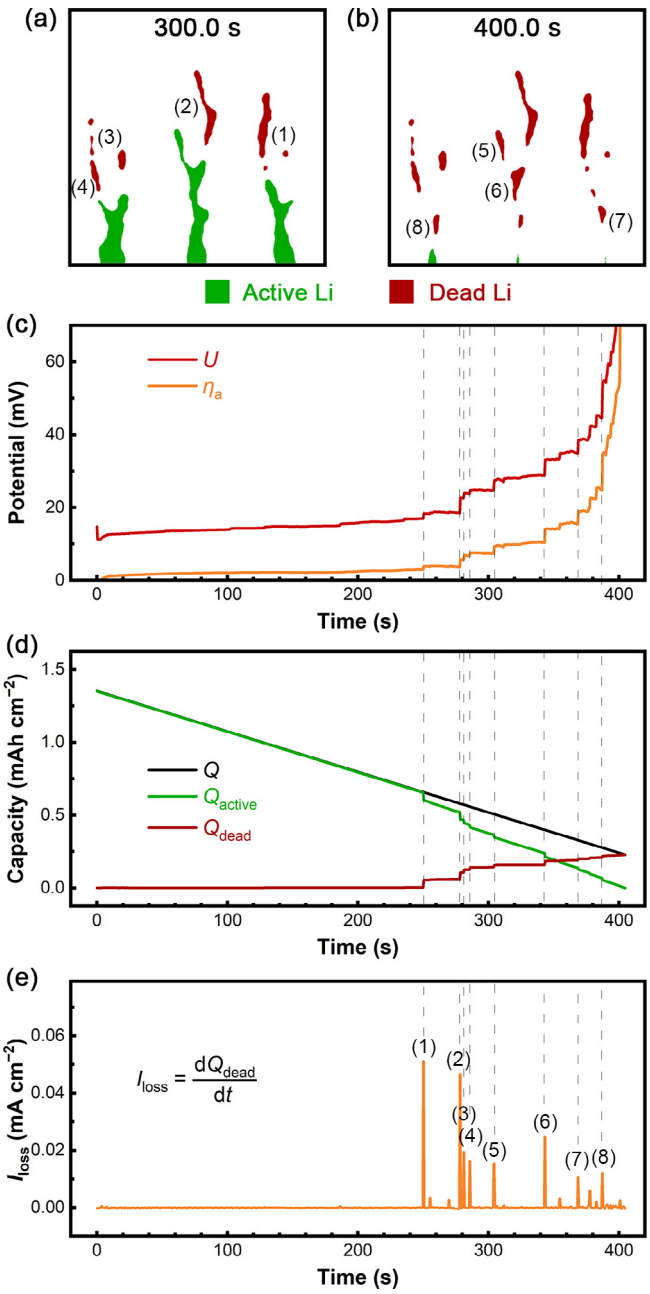

Fig. 4. Electrochemical properties during dead lithium formation. (a and b) The primary dead lithium pieces; (c) total voltage U and average activation overpotential η_a curves; (d) total lithium metal capacity Q, active lithium capacity Q_{active}, and dead lithium capacity Q_{dead} curves; (e) the capacity loss rate spectrum with multiple loss peaks corresponding to the primary dead lithium pieces.

4. Conclusions

A phase field model on the lithium stripping process with dead lithium formation was proposed for the first time. The galvanostatic charge and discharge conditions were also realized in this contribution, which can be matched with experimental results more conveniently and accurately, compared with the previous electrochemistry phase field models. With the proposed model,

the dead lithium formation process and its impacts on electrochemical performance were revealed.

1) The dead lithium formation reduces the active lithium metal surface area, and the increasing local Li ion concentration during lithium stripping together significantly increases the activation overpotential and cell polarization.
2) The dead lithium formation is directly responsible for the loss of cycle capacity. The phase field theory reveals the correspondence between the polarization curve and the capacity loss peak, and can realize the quantitative calculation of the Coulombic efficiency.

The dead lithium formation model proposed here is also of guiding significance for the simulation of material inactivation caused by fracture in other batteries. Besides, in order to obtain more instructive quantitative rules for the design of practical lithium metal batteries, large amounts of efforts on model adjustment are still required, such as the self-adapting description on the active state of local lithium metal. Furthermore, how material properties and charge–discharge conditions affect the formation process of dead lithium also needs to be further explored.

The phase field theory can carry out detailed and accurate quantitative exploration of the dead lithium formation process, and even other energy chemistry mechanisms on lithium metal batteries, from a perspective that was difficult to penetrate by routine experimental methods. The investigation on the mechanism of the lithium stripping process helps to further develop lithium metal batteries with high cycle efficiency and long lifespan.

Declaration of competing interest

The authors declare that they have no known competing financial interests or personal relationships that could have appeared to influence the work reported in this paper.

Acknowledgments

This work was supported by the National Natural Scientific Foundation of China (22109011) and the China Postdoctoral Science Foundation (BX20200047, 2021M690380).

Appendix A. Supplementary data

Supplementary data to this article can be found online at https://doi.org/10.1016/j.jechem.2021.12.020.

References

[1] C. Yan, H. Yuan, H.S. Park, J.-Q. Huang, J. Energy Chem. 47 (2020) 217–220.
[2] X.-B. Cheng, R. Zhang, C.-Z. Zhao, Q. Zhang, Chem. Rev. 117 (2017) 10403–10473.
[3] J. Xiao, Science 366 (2019) 426–427.
[4] M. Gao, H. Li, L. Xu, Q. Xue, X. Wang, Y. Bai, C. Wu, J. Energy Chem. 59 (2021) 666–687.
[5] Q.K. Zhang, X.Q. Zhang, H. Yuan, J.Q. Huang, Small Sci. 1 (2021) 2100058.
[6] X.-R. Chen, B.-C. Zhao, C. Yan, Q. Zhang, Adv. Mater. 33 (2021) 2004128.
[7] H. Zhang, Y. Chen, C. Li, M. Armand, SusMat 1 (2021) 24–37.
[8] R. Wang, W. Cui, F. Chu, F. Wu, J. Energy Chem. 48 (2020) 145–159.
[9] X. Shen, X.Q. Zhang, F. Ding, J.Q. Huang, R. Xu, X. Chen, C. Yan, F.Y. Su, C.M. Chen, X.J. Liu, Q. Zhang, Energy Mater. Adv. 2021 (2021) 1205324.
[10] X. Zheng, L. Huang, X. Ye, J. Zhang, F. Min, W. Luo, Y. Huang, Chemistry 7 (2021) 2312–2346.
[11] R. Xu, X.-B. Cheng, C. Yan, X.-Q. Zhang, Y. Xiao, C.-Z. Zhao, J.-Q. Huang, Q. Zhang, Matter 1 (2019) 317–344.
[12] Y. Liu, Y. Zhai, Y. Xia, W. Li, D. Zhao, Small Struct. 2 (2021) 2000118.
[13] M. Wu, Y. Li, X. Liu, S. Yang, J. Ma, S. Dou, SmartMat 2 (2021) 5–11.
[14] Y. Han, B. Liu, Z. Xiao, W. Zhang, X. Wang, G. Pan, Y. Xia, X. Xia, J. Tu, InfoMat 3 (2021) 155–174.
[15] J. Liu, H. Yuan, X. Tao, Y. Liang, S.J. Yang, J.-Q. Huang, T.-Q. Yuan, M.-M. Titirici, Q. Zhang, EcoMat 2 (2020) e12019.
[16] L. Kong, C. Tang, H.-J. Peng, J.-Q. Huang, Q. Zhang, SmartMat 1 (2020) e1007.
[17] M. Yang, Y. Liu, A.M. Nolan, Y. Mo, Adv. Mater. 33 (2021) 2008081.
[18] Y. Shi, J. Wan, G.-X. Liu, T.-T. Zuo, Y.-X. Song, B. Liu, Y.-G. Guo, R. Wen, L.-J. Wan, Angew. Chem. Int. Ed. 59 (2020) 18120–18125.
[19] C.-B. Jin, X.-Q. Zhang, O.-W. Sheng, S.-Y. Sun, L.-P. Hou, P. Shi, B.-Q. Li, J.-Q. Huang, X.-Y. Tao, Q. Zhang, Angew. Chem. Int. Ed. 60 (2021) 22990–22995.
[20] B.Q. Li, X.R. Chen, X. Chen, C.X. Zhao, R. Zhang, X.B. Cheng, Q. Zhang, Research 2019 (2019) 4608940.
[21] X. Shen, X.-B. Cheng, P. Shi, J. Huang, X.-Q. Zhang, C. Yan, T. Li, Q. Zhang, J. Energy Chem. 37 (2019) 29–34.
[22] Y.M. Chen, Z.Q. Wang, X.Y. Li, X.H. Yao, C. Wang, Y.T. Li, W.J. Xue, D.W. Yu, S.Y. Kim, F. Yang, A. Kushima, G.G. Zhang, H.T. Huang, N. Wu, Y.W. Mai, J.B. Goodenough, J. Li, Nature 578 (2020) 251–255.
[23] M.J. Zachman, Z.Y. Tu, S. Choudhury, L.A. Archer, L.F. Kourkoutis, Nature 560 (2018) 345–349.
[24] C.-X. Zhao, W.-J. Chen, M. Zhao, Y.-W. Song, J.-N. Liu, B.-Q. Li, T. Yuan, C.-M. Chen, Q. Zhang, J.-Q. Huang, EcoMat 3 (2021) e12066.
[25] Y.-X. Yao, X.-Q. Zhang, B.-Q. Li, C. Yan, P.-Y. Chen, J.-Q. Huang, Q. Zhang, InfoMat 2 (2020) 379–388.
[26] S. Yuan, T. Kong, Y. Zhang, P. Dong, Y. Zhang, X. Dong, Y. Wang, Y. Xia, Angew. Chem. Int. Ed. (2021), https://doi.org/10.1002/anie.202108397.
[27] E.M. Hitz, H. Xie, Y. Lin, J.W. Connell, G.W. Rubloff, C.-F. Lin, L. Hu, Small Struct. 2 (2021) 2100014.
[28] Y.-W. Song, P. Shi, B.-Q. Li, X. Chen, C.-X. Zhao, W.-J. Chen, X.-Q. Zhang, X. Chen, Q. Zhang, Matter 4 (2021) 253–264.
[29] S. Li, Z. Li, L. Huai, M. Ma, K. Luo, J. Chen, D. Wang, Z. Peng, J. Energy Chem. 62 (2021) 179–190.
[30] X.-Q. Xu, R. Xu, X.-B. Cheng, Y. Xiao, H.-J. Peng, H. Yuan, F. Liu, J. Energy Chem. 56 (2021) 391–394.
[31] Y. Gao, F. Qiao, J. You, C. Shen, H. Zhao, J. Gu, Z. Ren, K. Xie, B. Wei, J. Energy Chem. 55 (2021) 580–587.
[32] K. Shi, Z. Wan, L. Yang, Y. Zhang, Y. Huang, S. Su, H. Xia, K. Jiang, L. Shen, Y. Hu, S. Zhang, J. Yu, F. Ren, Y.-B. He, F. Kang, Angew. Chem. Int. Ed. 59 (2020) 11784–11788.
[33] K. Zhang, F. Wu, K. Zhang, S. Weng, X. Wang, M. Gao, Y. Sun, D. Cao, Y. Bai, H. Xu, X. Wang, C. Wu, Energy Storage Mater. 41 (2021) 485–494.
[34] X.-R. Chen, C. Yan, J.-F. Ding, H.-J. Peng, Q. Zhang, J. Energy Chem. 62 (2021) 289–294.
[35] Y. Xiang, M. Tao, G. Zhong, Z. Liang, G. Zheng, X. Huang, X. Liu, Y. Jin, N. Xu, M. Armand, J.-G. Zhang, K. Xu, R. Fu, Y. Yang, Sci. Adv. 7 (2021) eabj3423.
[36] P. Shi, X.-B. Cheng, T. Li, R. Zhang, H. Liu, C. Yan, X.-Q. Zhang, J.-Q. Huang, Q. Zhang, Adv. Mater. 31 (2019) 1902785.
[37] C.C. Fang, J.X. Li, M.H. Zhang, Y.H. Zhang, F. Yang, J.Z. Lee, M.H. Lee, J. Alvarado, M.A. Schroeder, Y.Y.C. Yang, B.Y. Lu, N. Williams, M. Ceja, L. Yang, M. Cai, J. Gu, K. Xu, X.F. Wang, Y.S. Meng, Nature 572 (2019) 511–515.
[38] H. Sun, Q. Liu, J. Chen, Y. Li, H. Ye, J. Zhao, L. Geng, Q. Dai, T. Yang, H. Li, Z. Wang, L. Zhang, Y. Tang, J. Huang, ACS Nano (2021), https://doi.org/10.1021/acsnano.1021c04864.
[39] S. Xu, K.-H. Chen, N.P. Dasgupta, J.B. Siegel, A.G. Stefanopoulou, J. Electrochem. Soc. 166 (2019) A3456–A3463.
[40] C. Jin, T. Liu, O. Sheng, M. Li, T. Liu, Y. Yuan, J. Nai, Z. Ju, W. Zhang, Y. Liu, Y. Wang, Z. Lin, J. Lu, X. Tao, Nat. Energy 6 (2021) 378–387.
[41] L. Yu, J. Wang, Z.J. Xu, Small Struct. 2 (2021) 2000043.
[42] X.-R. Chen, Y.-X. Yao, C. Yan, R. Zhang, X.-B. Cheng, Q. Zhang, Angew. Chem. Int. Ed. 59 (2020) 7743–7747.
[43] H. Mao, W. Yu, Z. Cai, G. Liu, L. Liu, R. Wen, Y. Su, H. Kou, K. Xi, B. Li, H. Zhao, X. Da, H. Wu, W. Yan, S. Ding, Angew. Chem. Int. Ed. 60 (2021) 19306–19313.
[44] R. Zhang, X. Chen, X. Shen, X.-Q. Zhang, X.-R. Chen, X.-B. Cheng, C. Yan, C.-Z. Zhao, Q. Zhang, Joule 2 (2018) 764–777.
[45] X. Chen, Y.-K. Bai, X. Shen, H.-J. Peng, Q. Zhang, J. Energy Chem. 51 (2020) 1–6.
[46] X. Chen, X. Shen, T.-Z. Hou, R. Zhang, H.-J. Peng, Q. Zhang, Chemistry 6 (2020) 2242–2256.
[47] F. Hao, B.S. Vishnugopi, A. Verma, P.P. Mukherjee, J. Phys. Chem. C (2021), https://doi.org/10.1021/acs.jpcc.1021c06532.
[48] X. Shen, R. Zhang, X. Chen, X.B. Cheng, X. Li, Q. Zhang, Adv. Energy Mater. 10 (2020) 1903645.
[49] V. Yurkiv, T. Foroozan, A. Ramasubramanian, R. Shahbazian-Yassar, F. Mashayek, Electrochim. Acta 265 (2018) 609–619.
[50] Z. Hong, V. Viswanathan, ACS Energy Lett. 3 (2018) 1737–1743.
[51] Z. Mu, Z. Guo, Y.-H. Lin, Energy Storage Mater. 30 (2020) 52–58.
[52] Y. Lu, L. Chang, Y. Song, L. He, Y. Ni, Extreme Mech. Lett. 42 (2021) 101152.
[53] Q. Wang, G. Zhang, Y. Li, Z. Hong, D. Wang, S. Shi, npj Comput. Mater. 6 (2020) 176.
[54] M.Z. Bazant, Acc. Chem. Res. 46 (2013) 1144–1160.
[55] J.E. Guyer, W.J. Boettinger, J.A. Warren, G.B. McFadden, Phys. Rev. E 69 (2004) 021603.
[56] J.E. Guyer, W.J. Boettinger, J.A. Warren, G.B. McFadden, Phys. Rev. E 69 (2004) 021604.
[57] L. Chen, H.W. Zhang, L.Y. Liang, Z. Liu, Y. Qi, P. Lu, J. Chen, L.-Q. Chen, J. Power Sources 300 (2015) 376–385.
[58] L. Liang, L.-Q. Chen, Appl. Phys. Lett. 105 (2014) 263903.

[59] R. Zhang, X. Shen, X.-B. Cheng, Q. Zhang, Energy Storage Mater. 23 (2019) 556–565.
[60] Y. Ren, Y. Zhou, Y. Cao, J. Phys. Chem. C 124 (2020) 12195–12204.
[61] W. Mu, X. Liu, Z. Wen, L. Liu, J. Energy Storage 26 (2019) 100921.
[62] X. Shen, R. Zhang, S. Wang, X. Chen, C. Zhao, E. Kuzmina, E. Karaseva, V. Kolosnitsyn, Q. Zhang, Chin. J. Chem. Eng. 37 (2021) 137–143.
[63] X. Shen, R. Zhang, P. Shi, X. Chen, Q. Zhang, Adv. Energy Mater. 11 (2021) 2003416.
[64] J. Zhang, y. Liu, C. Wang, H. Tan, J. Electrochem. Soc. 168 (2021) 090522.
[65] H.H. Yan, Y.H. Bie, X.Y. Cui, G.P. Xiong, L. Chen, Energ. Convers. Manage. 161 (2018) 193–204.
[66] Z.J. Hong, V. Viswanathan, ACS Energy Lett. 4 (2019) 1012–1019.